

PNNL-32953

# **A Very High Temperature Lead Cooled Microreactor Concept using Advanced Materials and Thermophotovoltaics Direct Energy Conversion Technology**

**June 2022**

JJ Jenks  
Chad Painter  
Harold Adkins  
Dion Sunderland  
Randy Schwarz  
Sarah Suffield  
Bruce Bernacki  
Pete McGrail

## DISCLAIMER

This report was prepared as an account of work sponsored by an agency of the United States Government. Neither the United States Government nor any agency thereof, nor Battelle Memorial Institute, nor any of their employees, makes **any warranty, express or implied, or assumes any legal liability or responsibility for the accuracy, completeness, or usefulness of any information, apparatus, product, or process disclosed, or represents that its use would not infringe privately owned rights.** Reference herein to any specific commercial product, process, or service by trade name, trademark, manufacturer, or otherwise does not necessarily constitute or imply its endorsement, recommendation, or favoring by the United States Government or any agency thereof, or Battelle Memorial Institute. The views and opinions of authors expressed herein do not necessarily state or reflect those of the United States Government or any agency thereof.

PACIFIC NORTHWEST NATIONAL LABORATORY  
*operated by*  
BATTELLE  
*for the*  
UNITED STATES DEPARTMENT OF ENERGY  
*under Contract DE-AC05-76RL01830*

Printed in the United States of America

Available to DOE and DOE contractors from the  
Office of Scientific and Technical Information,  
P.O. Box 62, Oak Ridge, TN 37831-0062;  
ph: (865) 576-8401  
fax: (865) 576-5728  
email: [reports@adonis.osti.gov](mailto:reports@adonis.osti.gov)

Available to the public from the National Technical Information Service  
5301 Shawnee Rd., Alexandria, VA 22312  
ph: (800) 553-NTIS (6847)  
email: [orders@ntis.gov](mailto:orders@ntis.gov) <<https://www.ntis.gov/about>>  
Online ordering: <http://www.ntis.gov>

# **A Very High Temperature Lead Cooled Microreactor Concept using Advanced Materials and Thermophotovoltaics Direct Energy Conversion Technology**

June 2022

JJ Jenks  
Chad Painter  
Harold Adkins  
Dion Sunderland  
Randy Schwarz  
Sarah Suffield  
Bruce Bernacki  
Pete McGrail

Prepared for  
the U.S. Department of Energy  
under Contract DE-AC05-76RL01830

Pacific Northwest National Laboratory  
Richland, Washington 99354



## Abstract

Recently, significant advances have been made in designing high-temperature capable nuclear fuels. In parallel, important advances have occurred in design of nanophotonic structures (coatings) with ability to shape the frequencies of light being emitted from hot surfaces. In this project, we bring these materials advances together into a design for a new direct conversion nuclear powered system with high thermodynamic efficiency, inherent safety, and unprecedented reduction in size and weight relative to current designs. The concept involves using the heat generated from nuclear fission to raise the temperature of a selective thermal emitter to  $>800^{\circ}\text{C}$ . The selective emitter shifts the normal broad band emissions of light from its hot surface into the correct near- and mid-infrared bands that produce electricity with inexpensive photovoltaic cells. We have designed a new annular flow Lead Fast Reactor that minimizes overall reactor/power conversion footprint. The results indicate that the overall microreactor/power-system design offers a 2X reduction in size over existing technology that is based on the supercritical carbon dioxide reverse compression Brayton cycle. Additionally, the only moving part in our design is a circulation pump to cool the thermal photovoltaic panels.

## Acknowledgments

This research was supported by the Energy and Environmental Directorate (EED) Mission Seed, a Laboratory Directed Research and Development (LDRD) Program at Pacific Northwest National Laboratory (PNNL). The computational work was performed using PNNL Institutional Computing at Pacific Northwest National Laboratory. PNNL is a multi-program national laboratory operated for the U.S. Department of Energy (DOE) by Battelle Memorial Institute under Contract No. DE-AC05-76RL0-1830.

## Acronyms and Abbreviations

|                  |   |
|------------------|---|
| CAD              | computer aided design                                       |
| CFD              | computational fluid dynamics                                |
| DBR              | distributed Bragg reflector                                 |
| DOD              | United States Department of Defense                         |
| DOE-NE           | United States Department of Energy Office of Nuclear Energy |
| ENZ              | epsilon near zero   |
| HALEU            | high-assay, low-enriched uranium                            |
| IR               | infrared  |
| MCNP             | Monte Carlo N-particle                                      |
| MW               | megawatt  |
| MWe              | megawatt thermal  |
| MWt              | megawatt electric   |
| NASA             | National Aeronautics and Space Administration               |
| NTPV             | nuclear thermal photovoltaic                                |
| OTT              | optical topological transition                              |
| PhC              | photonic crystal  |
| PV               | photovoltaic  |
| sCO <sub>2</sub> | supercritical carbon dioxide                                |
| SMR              | small modular reactor                                       |
| T                | temperature   |
| TPP              | Tamm plasmon polaritons                                     |
| TPV              | thermophotovoltaic  |
| TRISO            | tri-structural isotropic                                    |
| UR               | uranium nitride   |
| YH               | yttrium hydride   |

## Contents

|   |     |
|---|-----|
| Abstract.....   | ii  |
| Acknowledgments.....  | iii |
| Acronyms and Abbreviations.....   | iv  |
| 1.0 Introduction .....  | 1   |
| 2.0 Advanced Selective Emitter Technology.....                          | 3   |
| 2.2 DBR TPP Design.....   | 4   |
| 2.3 Epsilon-Near-Zero (ENZ) Design.....                                 | 6   |
| 3.0 Reactor Concept .....   | 8   |
| 3.1 Core and Neutronics .....   | 8   |
| 3.2 Materials Selection.....  | 9   |
| 3.3 Thermal Hydraulics .....  | 9   |
| 3.4 Additional Design Considerations .....                              | 12  |
| 4.0 Conclusions.....  | 17  |
| 5.0 References.....   | 18  |
| Appendix A – A Molten-Lead Loop for Material and Component Testing..... | A.1 |
| Appendix B – Efficiencies Comparison.....                               | B.1 |

## Figures

|  |   |
|--|---|
| Figure 1. Microreactor with Brayton cycle.....   |   |
| Figure 2. Direct conversion NTPV concept.....  |   |
| Figure 3. Size and weight comparison versus microreactor core temperature of Brayton system and NTPV system.....   | 2 |
| Figure 4. Plot showing the radiance of a 1500°C and 1000°C blackbody (left) along with a normalized plot of the two blackbody curves (right).....                    | 3 |
| Figure 5. DBR TPP selective emitter structure showing the Si/SiO <sub>2</sub> DBR, Si spacer and TiN thin film layer at the base.....                                | 4 |
| Figure 6. The DBR TPP design with TiN base is shown plotted against the normalized blackbody curves for 1000°C and 1500°C cases. ....                                | 5 |
| Figure 7. Plots of the combined radiance of the blackbody radiation and selective emitter coating at 1000°C (left) and at 1500°C (right) for the DBR TPP design..... | 5 |
| Figure 8. The ENZ design with SiC/TiN unit cells is shown plotted against the normalized blackbody curves for 1000°C and 1500°C cases. ....                          | 6 |
| Figure 9. Plots of the combined radiance of the blackbody radiation and selective emitter coating at 1000°C (left) and at 1500°C (right) for the ENZ design. ....    | 6 |



Figure 10. Figure 1b from Dyachenko<sup>2</sup> summarizes the effectiveness of the ENZ film mated with low-bandgap PV devices (blue region).....7

Figure 11. Idealized core showing typical unit cell enrichment profiles in the three radial zones. ....9

Figure 12. LFR thermal hydraulics CAD geometry and radial cross section of mesh..... 10

Figure 13. LFR Thermal Hydraulics CAD Geometry (Left-Pressure, Middle-Temperature, Right-Temperature on inside of Downcomer).....

Figure 14. 1D temperature profile of external cylindrical surface of the outer shroud. .... 12

Figure 15. Fully encapsulated design concept..... 13

Figure 16. Power generation of NTPV compared to alternative power system. .... 13

Figure 17. Comparison of placing a radiative heat exchanger above the core versus enveloping the core with the PV shroud. .... 14

Figure 18. Brayton design versus NTPV encapsulated design ..... 14

Figure 19. Radiative heat exchanger above core comparison to Brayton system for 2 MWe. .... 15

Figure 20. PV encapsulated (enveloped) core comparison to Brayton system for 2 MWe. .... 15

**Tables**

Table 1. Results for LFR thermal hydraulics CFD model..... 11

## 1.0 Introduction

All current commercial fission reactor systems are designed around a 160 yr old steam cycle or Brayton cycle to produce power as shown in Figure 1. The Brayton cycle, although somewhat more efficient than subcritical steam cycle systems, still requires a myriad of expensive heat exchangers, turbine, compressors, etc. that severely constrain ability to reduce size and weight, improve reliability and robustness, and cost that are critical to achieving United States Department of Defense (DOD), National Aeronautics and Space Administration (NASA), and United States Department of Nuclear Energy (DOE-NE) mission goals for small modular reactors (SMRs) and microreactor power systems. Our nuclear thermal photovoltaic (NTPV) concept breaks this paradigm by eliminating the unavoidable thermodynamic losses, numerous unit operations, heavy and sensitive turbo-machinery inherent with current power conversion systems. Instead, power is generated with direct radiated light-to-electrons conversion via simple and inexpensive photovoltaic technology with virtually no moving parts to maintain or breakdown.

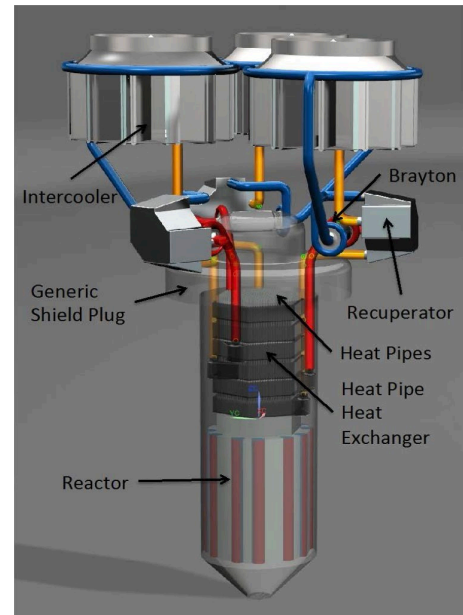


Figure 1. Microreactor with Brayton cycle.

A NTPV power system, shown in Figure 2, is a completely new concept for the nuclear energy sector but borrows from previous work in solar power generation. In solar applications, selective emitters are designed to shift the solar spectrum to enhance irradiance of the photovoltaic (PV) cell in the 1  $\mu\text{m}$  near-infrared (IR) wavelength matched to the bandgap of Si. In our NTPV power conversion system, the selective emitter needs to accomplish the same thing but with greater efficiency. This can now be done through a coupled-mode resonant layer structure design with refractory metals and oxides that significantly enhance emissivity in a targeted band. Because radiated power increases with temperature proportional to  $T^4$ , an extremely compact NTPV system would utilize an advanced reactor design that can generate temperatures  $>1200^\circ\text{C}$ . However, as shown in Figure 3, the power components for the NTPV system are significantly lighter and more compact than any additively manufactured Brayton power system at temperatures as low as  $800^\circ\text{C}$ . Hence the NTPV concept can have a significant impact even when leveraging more conventional reactor core designs using tri-structural isotropic (TRISO) fuel as an example. Fortunately, nuclear engineers have been

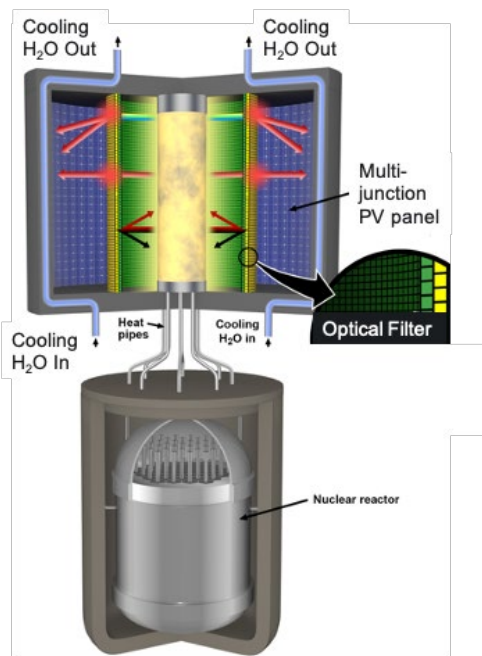


Figure 2. Direct conversion NTPV concept.

utilize an advanced reactor design that can generate temperatures  $>1200^\circ\text{C}$ . However, as shown in Figure 3, the power components for the NTPV system are significantly lighter and more compact than any additively manufactured Brayton power system at temperatures as low as  $800^\circ\text{C}$ . Hence the NTPV concept can have a significant impact even when leveraging more conventional reactor core designs using tri-structural isotropic (TRISO) fuel as an example. Fortunately, nuclear engineers have been

prolific in development of other innovative reactor core designs that can operate at temperatures where NTPV becomes even more advantageous. Our objective on this project was to assess feasibility of integrating one or more of these designs with a thermophotovoltaic (TPV) system.

The PV cells in any NTPV design must be protected from neutron and gamma radiation. In addition, the panels must have an active cooling system that maintains an average temperature of the PV panels at 100 °C. However, any cooling or shielding must not interfere with transmission of light in the effective wavelength region. This will likely require separation of the TPV array and reactor and a heat transfer method used to heat the selective emitter. However, this is not significantly different from conventional designs. Design of the selective thermal emitter for the advanced high-temperature capable design will require use of refractory materials such as W, Zr, Hf, Mo, etc.

and their corresponding oxides with sufficiently high melting temperature. This will constrain to some extent the ability to suppress emissions in the visible and far-IR bands that do not contribute to power generation with the PV array. However, ongoing research and development at PNNL was leveraged in designing selective emitters suitable for operation at these temperatures, which includes use of critically-coupled thin-film layers (resonant structures) that are optimized through machine learning algorithms. The optical filter design will draw upon commercially available hot IR mirrors and IR transparent glasses.

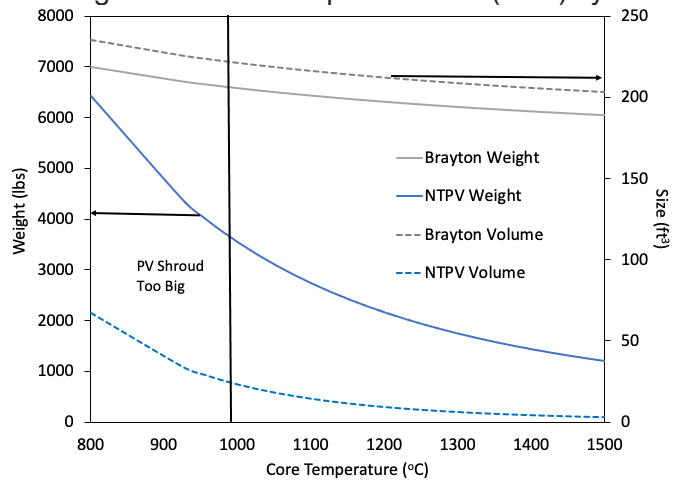


Figure 3. Size and weight comparison versus microreactor core temperature of Brayton system and NTPV system.

## 2.0 Advanced Selective Emitter Technology

The NPTV project seeks to directly produce electricity by harvesting the radiant heat from an operating nuclear reactor and efficiently thermally radiating a TPV cell to efficiently match the peak wavelength of the graybody emission from the reactor to the bandgap of the cell. Presently, two temperatures of reactor operation are envisioned: 1000°C and 1500°C. Blackbody plots of these two temperatures are shown in Figure 4: one in units of radiance, and the other normalized to better illustrate the peak emission wavelength relationship between the two temperatures.

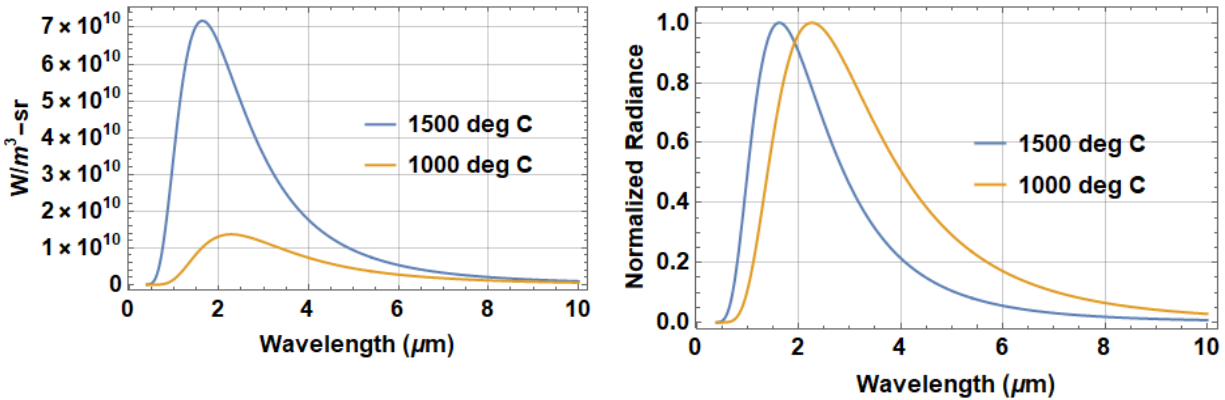


Figure 4. Plot showing the radiance of a 1500°C and 1000°C blackbody (left) along with a normalized plot of the two blackbody curves (right).

The peak emission wavelength is given by the Wien displacement law, which states that the blackbody curve will peak at different wavelengths for different temperatures, and this wavelength peak is inversely proportional to temperature. In Eq. 1  $b$  is a constant of proportionality called Wien’s displacement constant with a value of 2897.771955 μm-K.

$$\lambda_{peak} = \frac{b}{T} \tag{1}$$

Therefore at 1000°C the peak emission wavelength is 2.27606 μm and at 1500°C the peak wavelength blue shifts to 1.63425 μm.

The Stefan-Boltzmann law describes the total power per unit area emitted over all wavelengths over all time and is proportional to the temperature to the 4<sup>th</sup> power. In Eq. 2,  $k$  is Boltzmann’s constant,  $h$  is Planck’s constant, and  $c$  is the velocity of light.

$$P = \sigma T^4$$

$$\sigma = \frac{2\pi^5 k^4}{15c^2 h^3} \tag{2}$$

Therefore, for our two temperature examples, at 1000°C, the power per unit area is 148.775 kW/m<sup>2</sup> and at 1500°C, it increases to 559.748 kW/m<sup>2</sup>, or 3.76 times greater than that emitted at 1000°C for the same emissivity.

The goal of the optical design will be to extract the most radiant portions of the blackbody curve at these two temperatures to emit that energy that best matches the bandgap of the TPV device

and generate electricity. Several approaches to designing selective emitter surfaces that tailor their emission with respect to the blackbody emission to achieve this goal are explained in the remainder of this document along with design examples.

## 2.1 Selective Emitter Coatings

A selective emitter coating requires that a specified emittance is produced over a certain wavelength range. Kirchoff's Law states that at thermal equilibrium, the amount of heat radiated by an object equals the power absorbed. For any material irradiated by thermal energy the relationship in Eq. 3 must be true invoking conservation of energy for unity input. A material such as a metal will not transmit electromagnetic energy making  $t$  or transmitted energy zero, so  $1-r$  must equal  $a$ , the energy absorbed, and whatever is absorbed, must be radiated, or emitted. Therefore, if a coating can be engineered to have very low reflectance over the wavelength band of interest, the amount absorbed, and hence, emittance must be high.

$$1 = a + r + t \quad (3)$$

Two practical candidates that will be considered will be a multi-layer coating consisting of a distributed Bragg reflector (DBR) structure with a spacer and metal base (TiN) that excites Tamm plasmon polaritons (TPP) between the DBR and TiN base to affect the selective emitter behavior, and a 1-D metamaterial consisting of repeated dielectric/metal pairs. Photonic crystal (PhC) surfaces are also often considered for selective emitter surfaces, but although they have the advantage of a monolithic material construction with better temperature performance (there are no dissimilar materials to cause stress and failure via delamination), they require advanced lithography capable of sub-wavelength features not currently available at PNNL, so will not be considered here.

## 2.2 DBR TPP Design

This design was described in a paper by Yang *et al*<sup>1</sup> and consists of a DBR pair of Si/SiO<sub>2</sub>, a Si spacer, and a TiN thin film at the base. A schematic of the stack is shown below from Yang *et al*<sup>1</sup>. The published design exhibited selective emittance centered at 4 μm so this design must be modified, and the center wavelength shifted to 2 μm.

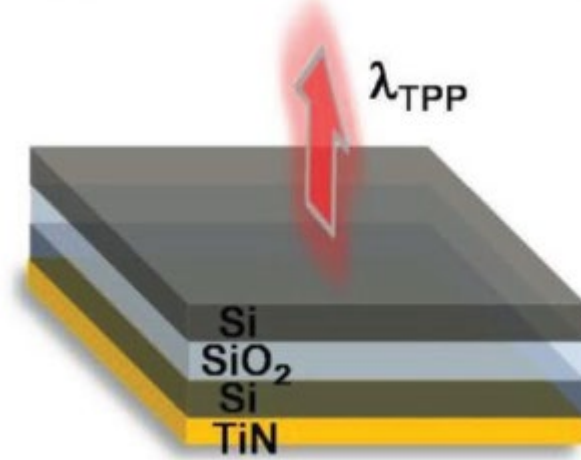


Figure 5. DBR TPP selective emitter structure showing the Si/SiO<sub>2</sub> DBR, Si spacer and TiN thin film layer at the base.

One candidate design centered at 2  $\mu\text{m}$  is shown in Figure 5 with Si/SiO<sub>2</sub> thickness of 300/280 nm, and the Si space layer with thickness 120 nm. The TiN layer is 200 nm; its thickness is not critical so long as it is “thick enough” to be opaque. The bandpass of the selective emitter design is shown in Figure 6 plotted along with the normalized blackbody curves.

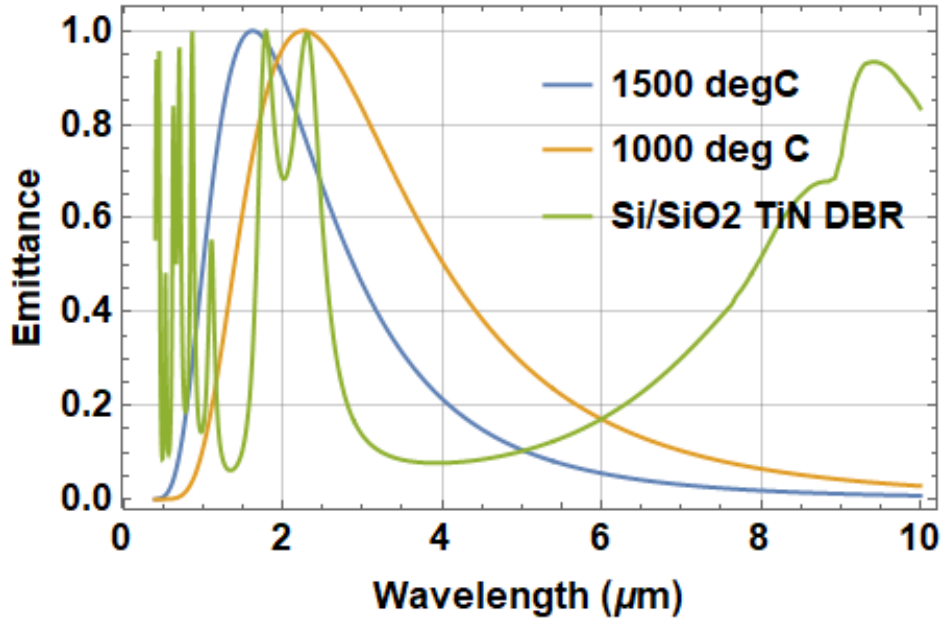


Figure 6. The DBR TPP design with TiN base is shown plotted against the normalized blackbody curves for 1000°C and 1500°C cases.

If the tailored emittance function is multiplied by each blackbody curve the selective emittance of the thermal emission at 1000°C and 1500°C can be evaluated and these results are shown in Figure 7. Note that the largest radiance of the blackbody curves is selectively emitted to a notional TPV device with a bandgap centered at 2  $\mu\text{m}$  (0.62 eV).

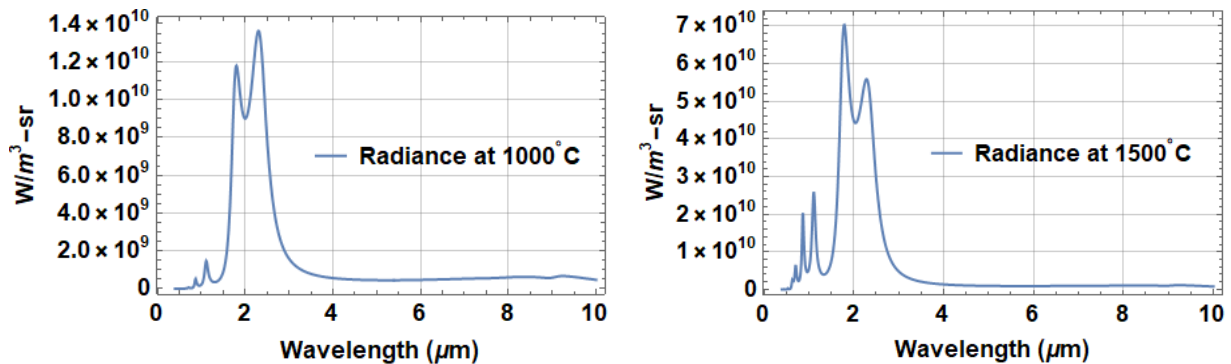


Figure 7. Plots of the combined radiance of the blackbody radiation and selective emitter coating at 1000°C (left) and at 1500°C (right) for the DBR TPP design.

### 2.3 Epsilon-Near-Zero (ENZ) Design

The ENZ design is a 1-D metamaterial consisting of a repeated pair of dielectric/metal layers. In the paper by Dyachenko<sup>2</sup>, the ENZ derives its name by engineering the thicknesses of the metal and dielectric layers such that at the optical topological transition (OTT), the relative permittivities (or dielectric constant  $\epsilon$ ) are equal and enhanced emittance occurs. An example that uses a dielectric/metal pair of SiC/TiN is shown below with thickness of 150/20 nm for the dielectric/metal plotted against the normalized blackbody radiance for the 1000°C and 1500°C temperatures in Figure 8. Four of these dielectric/metal pairs are needed to achieve this performance. This is a broader response than that of the DBR-TPP design, but the use of refractory metals along with the high melting point of SiC makes this design capable of extremely high temperature operation.

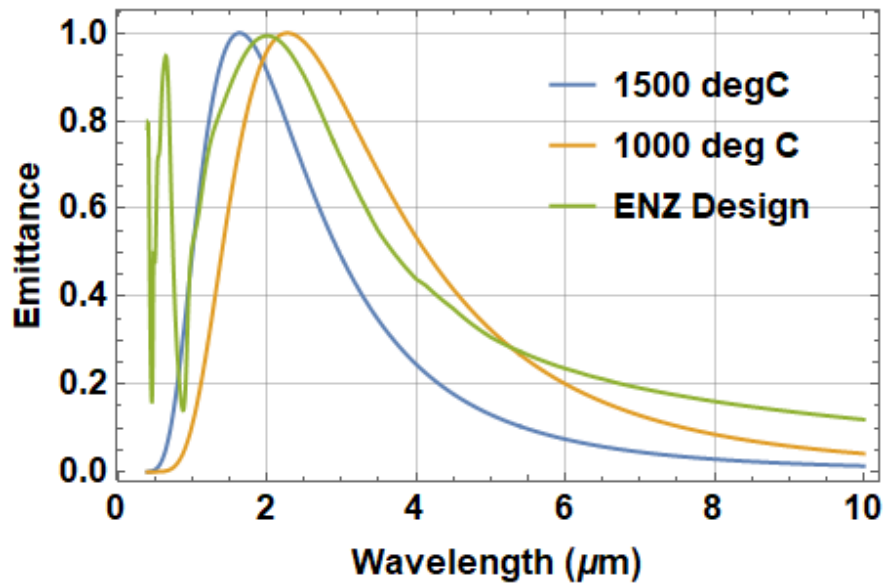


Figure 8. The ENZ design with SiC/TiN unit cells is shown plotted against the normalized blackbody curves for 1000°C and 1500°C cases.

If we now multiply the selective emitter response with the blackbody radiance plots, we obtain the results shown in Figure 9, which shows nearly ideal emittance of both of the blackbody curves.

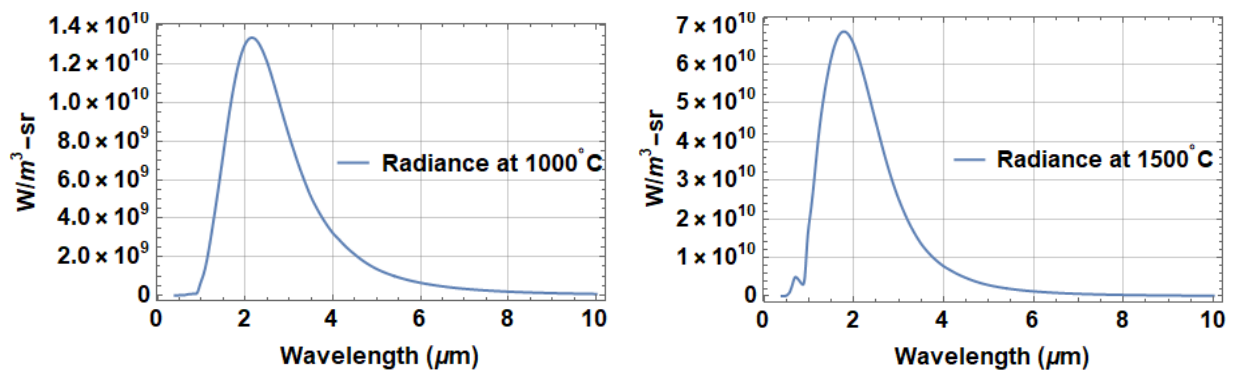


Figure 9. Plots of the combined radiance of the blackbody radiation and selective emitter coating at 1000°C (left) and at 1500°C (right) for the ENZ design.

Two candidate selective emitter approaches were introduced for the NTPV concept to directly convert heat from a nuclear reactor into electricity using TPV devices. These methods included the DBR-TPP design using a single DBR pair of Si/SiO<sub>2</sub> with Si spacer and TiN layer to make possible the TPP, as well as a 1-D metamaterial using repeated pairs of SiC/TiN to create an epsilon-near-zero film. The DBR-TPP design achieved a narrow bandwidth design, while the ENZ design bandwidth is broader. A figure from Dyachenko<sup>2</sup> shown in Figure 10 nicely summarizes the approach and the overlap of the selective emitter with that of low-bandgap TPV devices such as those constructed of InGaAsSb<sup>3</sup>. Ultimately, optimization of the selective emitter surface will depend on the band gap of the TPV device chosen to ensure that only light within the sensitive region of the band gap that can contribute to the generation of electricity is allowed to illuminate the device to eliminate unproductive heating of the device and thus to ensure the most efficient operation.

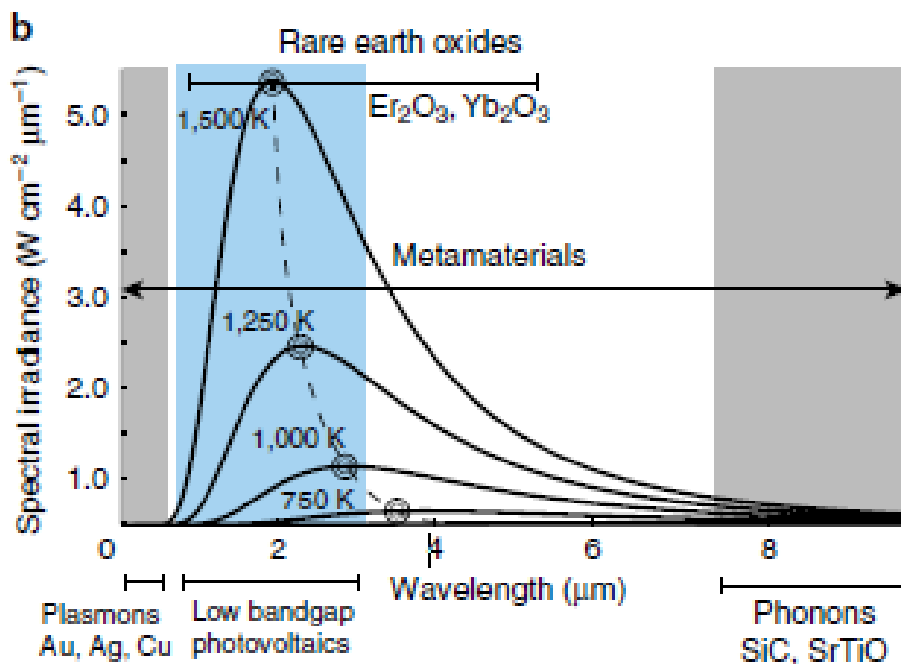


Figure 10. Figure 1b from Dyachenko<sup>2</sup> summarizes the effectiveness of the ENZ film mated with low-bandgap PV devices (blue region).



## 3.0 Reactor Concept

The lead-cooled very high temperature microreactor core (see Figure 11) which enables the efficient thermal photovoltaic direct energy power conversion wrapper shell is a fast spectrum design delivering approximately 4.3 MWt of thermal power with a nominal inlet and outlet temperature of 1,400°C and 1500°C, respectively. The active core (including reflector) radius is ~50 cm and the active core height (comprised of enriched UN<sup>4,5,6,7</sup>) is ~67.7 cm with ~16 cm natural UN blankets on top and bottom. The cladding material is a dilute Mo-alloy<sup>8,9,10</sup> which may also be used for core shroud, core support and containment structures. The design life is 7 years, with a core average burnup of 1.85 GWd/tUN, or 1.96 GWd/tU.

### 3.1 Core and Neutronics

A simple core was modeled using Monte Carlo N-particle (MCNP) which assumed approximately 5,800 high-assay, low-enriched uranium (HALEU) nitride fuel pins with axial and radial enrichment zoning to flatten power peaking and with axial and radial natural uranium nitride (UN) reflectors and a yttrium hydride (YH ~ YH<sub>1.8</sub>)<sup>11</sup> blanket to minimize leakage. The total mass of UN is approximately 5,947 kg, of which 3,212 kg UN is enriched (HALEU) and 2,735 kg is natural UN. The core is divided into three radial zones: inner enriched zone (~35%) with a slightly reduced enrichment for power peaking control, outer enriched zone (~55%) fully enriched, and an outer reflector (10%) of naturally enriched UN. The axial blankets are the same for all three regions.

Shielding of neutrons and gamma radiation are provided by the axial and radial (reflector) blankets surrounding the enriched inner and outer enriched zones in the core. The Mo-alloy cladding and liquid lead coolant also provide gamma shielding. The blankets also reduce neutron leakage, which is approximately 5% with a photon leakage of 0.08%. Neutron may be reduced further by special assembly lattice designs on the periphery, however, the assemblies would require special radial zoning.

Outside of the radial reflector, a 1-cm shroud of Mo-alloy provides a vessel to maintain coolant flow in the core. A 2-cm layer of YH is provided to thermalize fast neutrons. A downcomer area of lead provides a path for the lead coolant to return to the core. Forming the outer part of the downcomer is a reactor containment vessel consisting of a 3-cm thick wall of Mo-alloy.

The design is conceptual (currently the  $k_{\text{eff}}$  is ~1.0305), and no efforts has been made to model control rods and/or reactivity control systems. Details to be considered are the fuel assembly geometry, with ducts, and the number and placement of control rods.

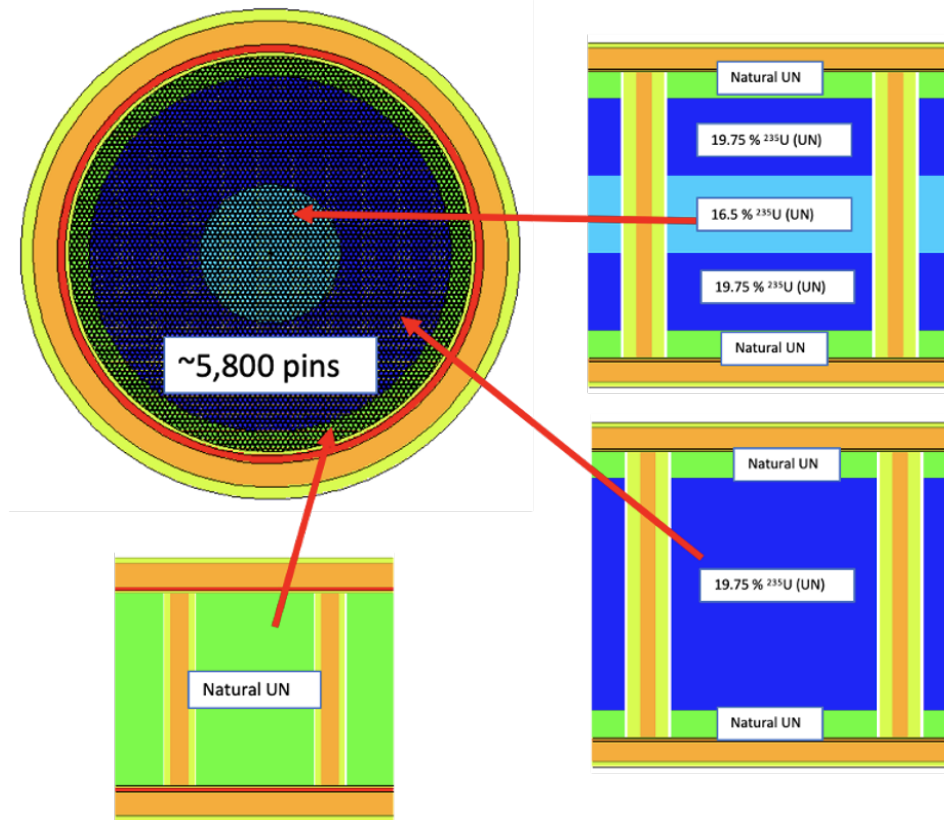


Figure 11. Idealized core showing typical unit cell enrichment profiles in the three radial zones.

### 3.2 Materials Selection

UN fuel was selected due to its high thermal conductivity and density ( $14.3 \text{ g/cm}^3$  theoretical density at room temperature), which allows for a compact core and relatively low fuel temperature, which is critical given the high coolant temperature. It is anticipated that the fuel pellet density will be 0.95 of theoretical, and the nitrogen will be enriched in  $^{15}\text{N}$ .

The fuel pellets are clad in a dilute Mo-based alloy selected for its high melting point, high strength and creep resistance at temperature, compatibility with UN and compatibility with the coolant. A Mo-alloy is considered preferable to a Nb alloy based on strength, and a Ta-alloy based on neutronic efficiency. The coolant is lead (Pb) with the possibility of a eutectic Pb-alloy.

The core barrel, core support structures and containment vessel will be the same Mo-alloy. The outer structure supporting the PV power conversion bank can be compatible steel with appropriate transition pieces of compatible materials.

### 3.3 Thermal Hydraulics

A computational fluid dynamics (CFD) model of the LFR system was constructed using the commercial software STAR-CCM+ (Siemens PLM Software 2021). The geometry for the CFD model was generated using the commercial computer-aided design (CAD) software SolidWorks (Dassault Systems SolidWorks Corp., 2020). The geometry includes a lead core region, 1 cm thick inner shroud, 2 cm thick reflector next to the inner shroud, and 3 cm thick outer shroud.

The core region has a radius of 50 cm and a total axial length of 116.56 cm. The axial length included the core height, a top and bottom axial reflector, and a non-active region at the top. The fuel pins have a pitch of 1.25 cm. For computational efficiency the model geometry was constructed to be a quarter symmetry model. Figure 12 shows the CAD geometry for the thermal hydraulics model. The lead region is shown in orange, the reflector in red, and the shrouds in green.

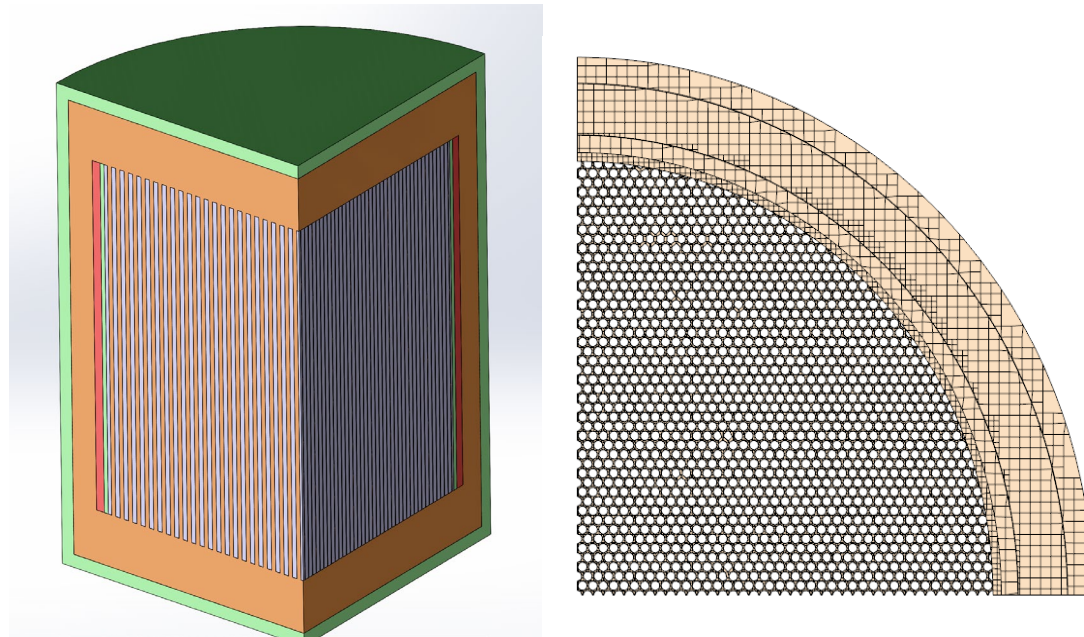


Figure 12. LFR thermal hydraulics CAD geometry and radial cross section of mesh.

The SolidWorks geometry was imported into STAR-CCM+. The geometry was then meshed into regions connected by interface boundaries, resulting in a hexahedral volume mesh for each component. Along each wall/fluid interface, the mesh contains prism cell layers to improve the accuracy of the flow solution near the walls. The prism cell layer consists of orthogonal prismatic cells adjacent to the wall boundaries.

A heat load was applied to the axial core boundaries of the lead region. The heat load was based on a radial and axial profile provided by the MCNP model. For the quarter symmetry model, the total heat load summed to 1.07 MW (one-fourth of the total 4.29 MW heat load). Temperature boundaries were applied to the inlet and outlet of the axial core region and were set to 1400°C and 1500°C respectively. The external boundaries of the outer shroud were modeled with an environmental boundary condition that allowed for radiation to the PV panels. The environmental boundary assumed an environment/PV panel temperature of 100°C.

Laminar flow was assumed in the lead liquid region. The Boussinesq model was applied to this laminar flow region to provide a buoyancy source term. The model was run as a steady state analysis and results are shown in Table 1. Figure 13 shows a pressure and temperature contour plot at the symmetry plane as well as an isometric thermal profile on the inside of the downcomer.

Table 1. Results for LFR thermal hydraulics CFD model

| CFD Model Result                                    | Value    | Unit              |
|---|----------|-------------------|
| Pressure drop across core                           | 22501    | Pa                |
| Average velocity through core region                | 4.92E-02 | m/s               |
| Average flowrate through core region                | 3.72E-03 | m <sup>3</sup> /s |
| Mass flow through the core                          | 15.3     | kg/s              |
| Average temperature of outside surface of downcomer | 1684     | K                 |
| Average temperature of inside surface of downcomer  | 1773     | K                 |

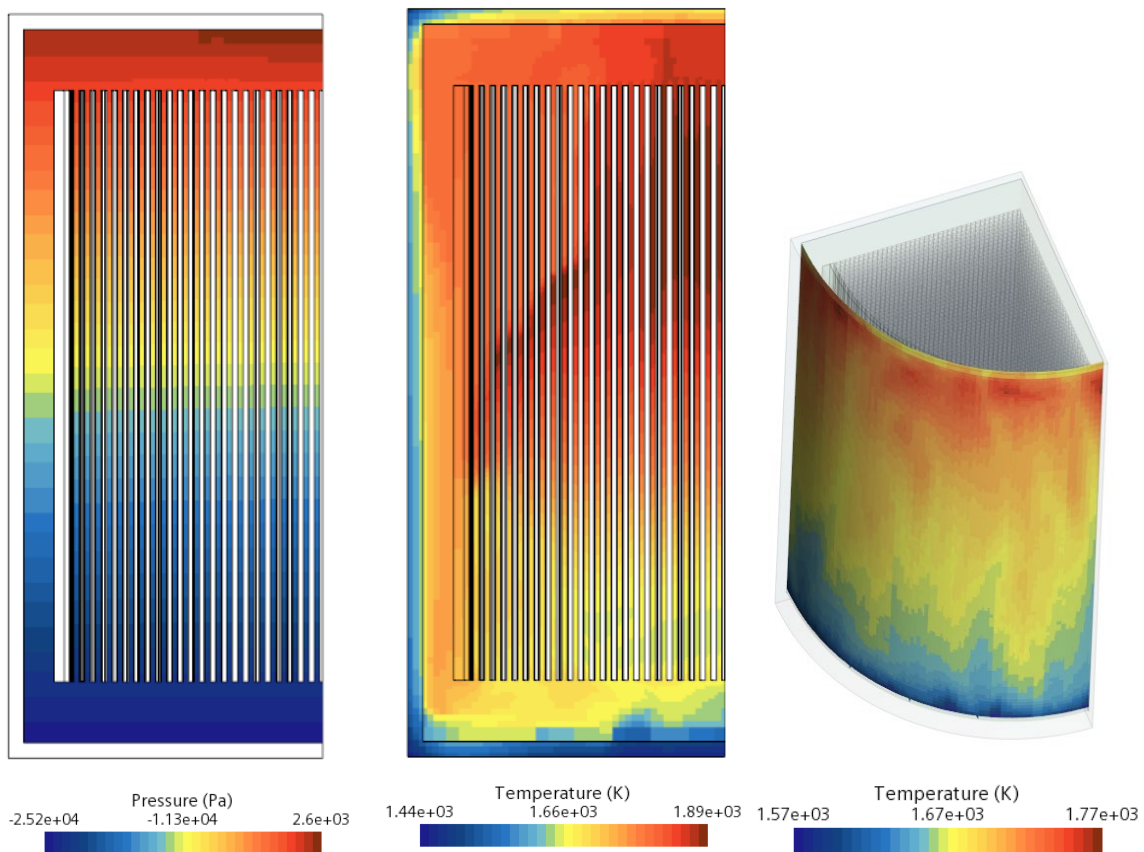


Figure 13. LFR Thermal Hydraulics CAD Geometry (Left-Pressure, Middle-Temperature, Right-Temperature on inside of Downcomer).

A 1D temperature profile plot was generated along the external cylindrical surface of the outer shroud in the axial direction to characterize the temperature profile. This surface radiates to the PV panels. Figure 14 shows the resulting temperature profile in the axial direction.

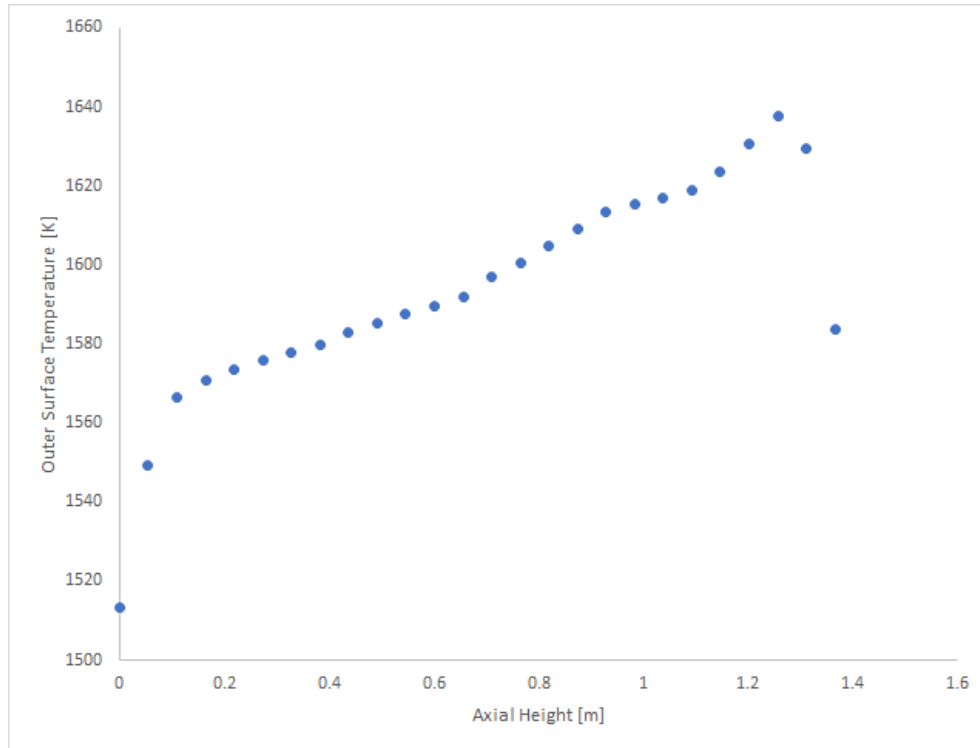


Figure 14. 1D temperature profile of external cylindrical surface of the outer shroud.

### 3.4 Additional Design Considerations

The challenge was to complete a design that integrates and protects the TPV system with a reactor. An initial design was completed that shows the most promise for very high temperature reactors, and it's a system that generates megawatts (MWs) of electricity per square meter of PV area. The fully encapsulated concept is shown in Figure 15 and can be a drop-in standalone power system that has a life of 7-10 years. The lead-cooled very high temperature microreactor core which enables the efficient thermal photovoltaic direct energy power conversion wrapper shell is a fast spectrum design delivering approximately 4.3 MWt of thermal power with a nominal inlet and outlet temperature of 1400 and 1500°C, respectively, as previously discussed.

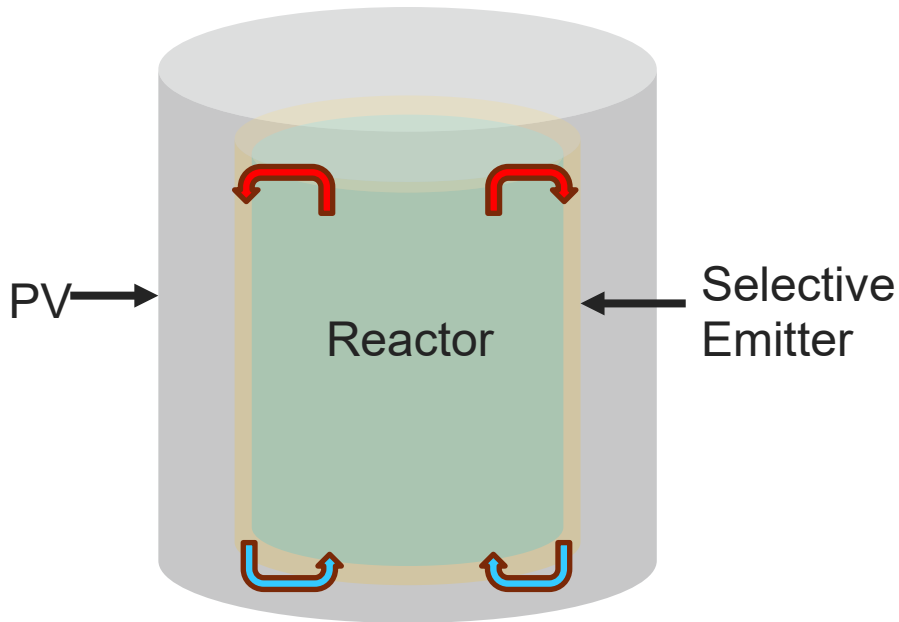


Figure 15. Fully encapsulated design concept.

Figure 16 shows a plot of power versus temperature for Brayton and NTPV power systems. Following the black NTPV line starting at 800 °C, the PV shroud is elongated beyond that of the reactor to generate at least 2 MWe. In other words, at lower temperatures the conversion efficiency is lower and therefore the PV shroud must be bigger. At just over 1100 °C surface temperature (200 °C below the reactor core design), the PV panel is the same length as the reactor. Beyond 1100 °C the PV shroud remains constrained by the geometry of the reactor in order to fully encapsulate it, and thus the power goes up with temperature as shown. At the average reactor outside surface temperature from the LFR, the NTPV system can generate nearly 2X that of a conventional power conversion system.

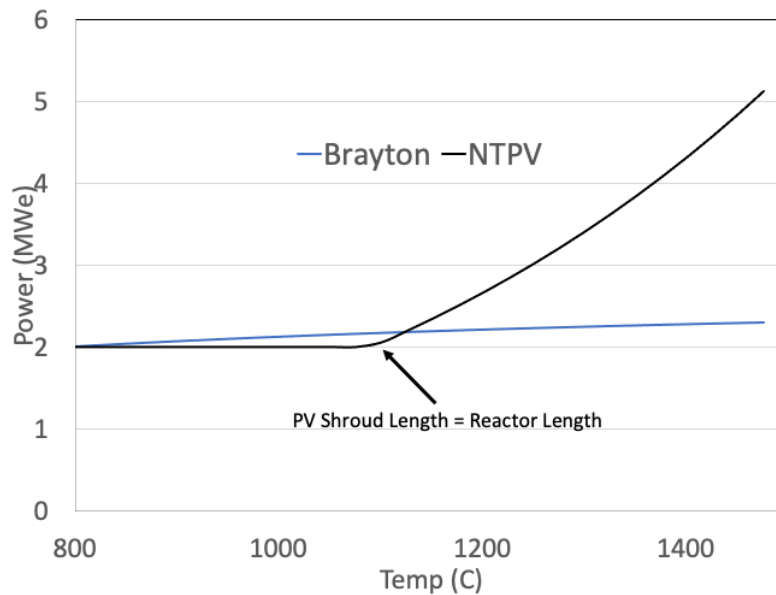


Figure 16. Power generation of NTPV compared to alternative power system.

Figure 17 shows the effect of placing a radiative heat exchanger above the core with a PV shroud around it as depicted in Figure 2. In order to fit into a standard roughly 9 ft by 9 ft (opening) shipping container the minimum operating temperature would need to be nearly 1000 °C. In addition, the overall core/power-system length would be much more than an encapsulated design.

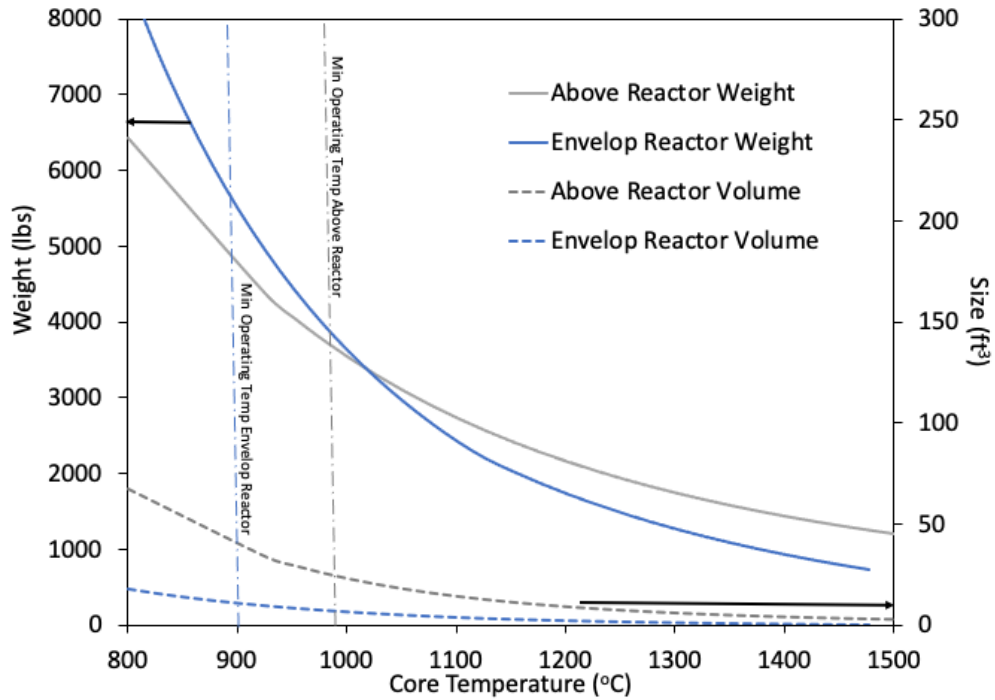


Figure 17. Comparison of placing a radiative heat exchanger above the core versus enveloping the core with the PV shroud.

An encapsulated design would fit inside a standard shipping container at around 900 °C. At the core design operating temperatures considered in the previous sections, this would allow for two NTPV systems to occupy the volume of one Brayton system as shown in Figure 18.

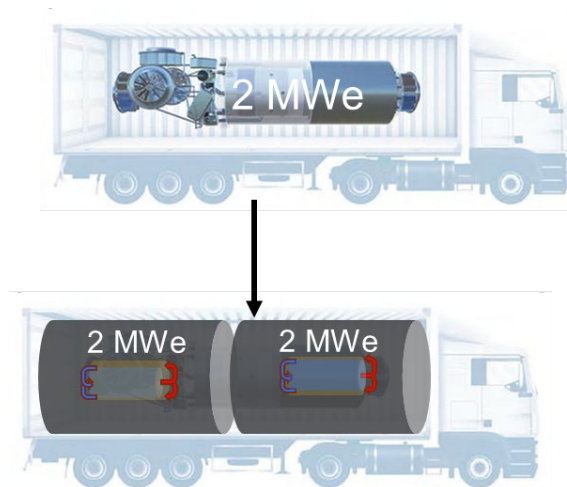


Figure 18. Brayton design versus NTPV encapsulated design

Figure 19 and Figure 20 show a comparison of the two PV shroud schemes compared to a Brayton system for 2 MWe power generation.

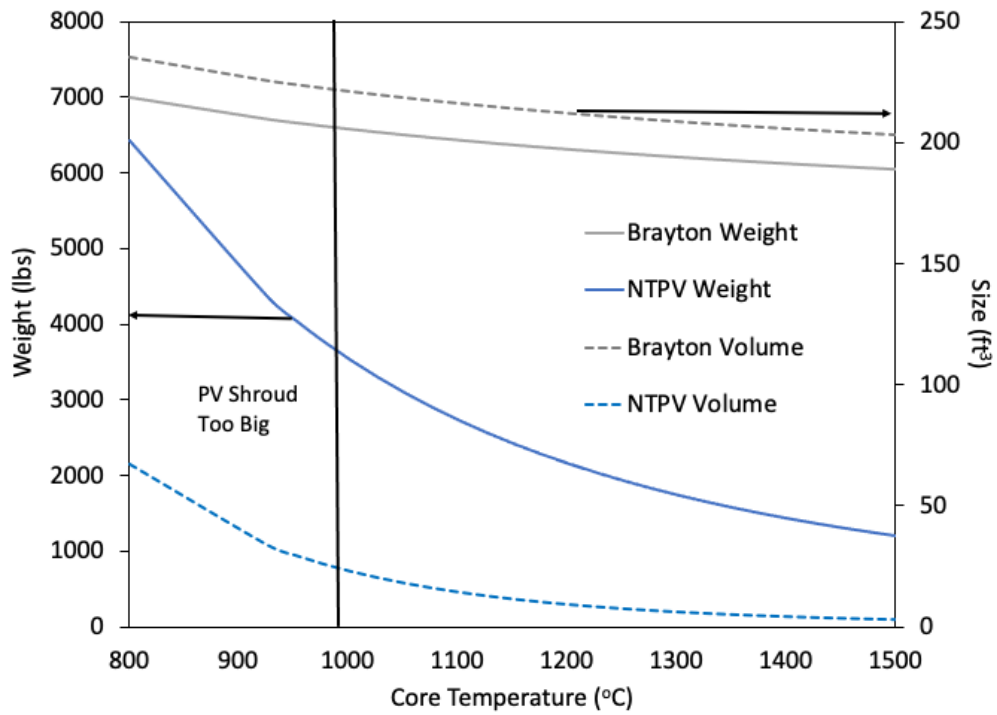


Figure 19. Radiative heat exchanger above core comparison to Brayton system for 2 MWe.

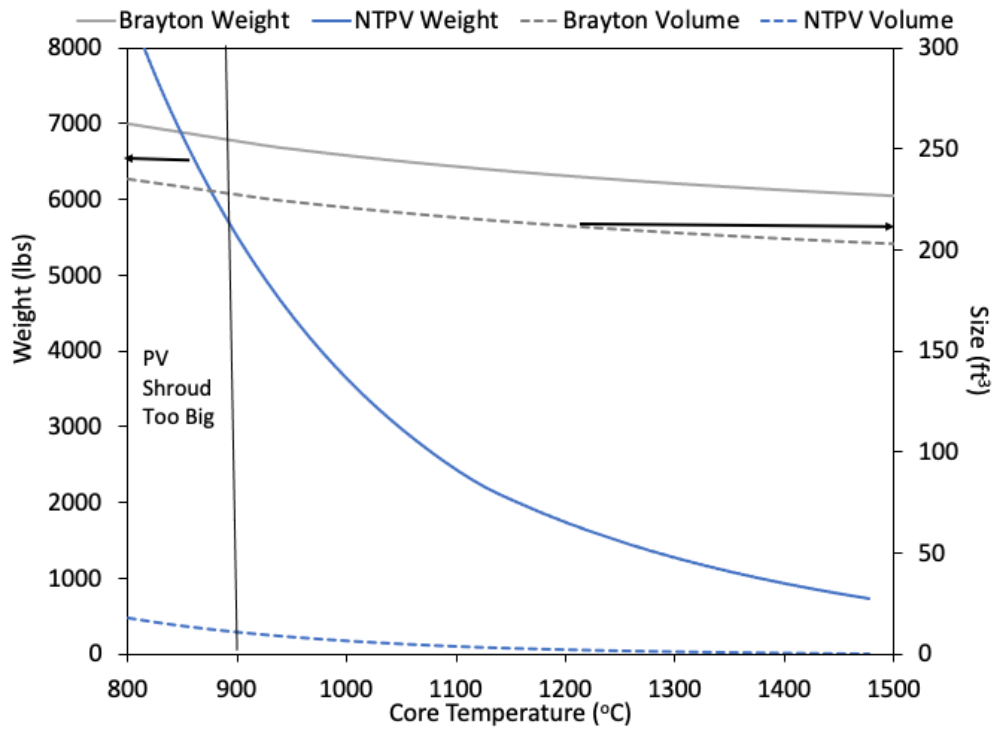


Figure 20. PV encapsulated (enveloped) core comparison to Brayton system for 2 MWe.



The use of lead as a coolant is not trivial and there are several details not mentioned in this report to consider and are detailed in Appendix A. Appendix B shows a plot of Carnot, Brayton, and NTPV efficiencies in addition to the Landsberg limit. Brayton and NTPV efficiencies were used in calculating overall power component sizes shown in the size/weight figures above.

## 4.0 Conclusions

In summary, a novel LFR was designed to radiate energy to a cooled thermophotovoltaic shroud that can produce the same amount of power as a sCO<sub>2</sub> Brayton system at surface temperatures of 800 °C and above. This is made possible due to selective emitters that are designed to radiate light into the narrow bandgap region specific to generating an electron-hole-pair in inexpensive commercially available thermophotovoltaic cells comprised of no more than 3 semi-conductors. If core temperatures were raised to 1400 °C as in this study, the NTPV system would occupy ½ the footprint of a Brayton system operating at the same temperature. LFR technology with annular flow offers unique advantages including additional shielding and zero moving parts. The flow of the lead coolant occurs through natural convection. Thermal hydraulics indicate that a coolant lead flow velocity of 5 cm/s is achieved by natural convection and is sufficient to keep the molybdenum encapsulated core cool while radiating 4.3 MWt from the selective emitter coated outermost portion of the core downcomer to produce at least 2 MWe power. The only moving part of the entire NTPV system is a cooling pump used to circulate fluid to maintain the panels at 100 °C.

## 5.0 References

---

1. Z-Y. Yang et al, "Narrow-Band Thermal Emitter with Titanium Nitride Thin Film Demonstrating High Temperature Stability," *Adv. Optical Mater.*, 1900982 (2020); <http://dx.doi.org/10.1002/adom.201900982>
2. P.N. Dyachenko et al, "Controlling thermal emission with refractory epsilon-near-zero metamaterials via topological transitions," *Nature Communications*, 7:11809 (2015); <http://dx.doi.org/10.1038/ncomms11809>
3. R.S. Tuley and R.J. Nicholas, "Band gap dependent thermophotovoltaic device performance using the InGaAs and InGaAsP material system," *J. Appl. Phys.* 108, 084516 (2010); <https://doi.org/10.1063/1.3488903>
4. C.M. Cox, D.S. Dutt, R.A. Karnesky, "Fuel Systems for Compact Fast Space Reactors," Chapter 36, *Space Nuclear Power Systems, Vol. 2*, M.S. El-Genk and M.D. Hoover, Eds., Orbit Book Co., 1984, pp. 301-306
5. A.W. Cronenberg and W. A. Ranken, "Irradiation Effects on Fuels for Space Reactors," Chapter 37, *Space Nuclear Power Systems, Vol. 2*, M.S. El-Genk and M.D. Hoover, Eds., Orbit Book Co., 1984, pp. 307-316
6. D. S. Dutt, C. M. Cox, R. A. Karnesky, M. K. Millhollen, "Performance and Testing of Refractory Alloy-Clad Fuel Elements for Space Reactors," HEDL-SA-3347, 20th Intersociety Energy Conversion Engineering Conference August 18-23.1985, Miami Beach, FL
7. Bruce J. Makenas, Dean M. Paxton, Swaminathan Vaidyanathan and Carl W. Hoth, "SP-100 Fuel Pin Performance: Results from Irradiation Testing," *AIP Conference Proceedings* 301, 403 (1994); <https://doi.org/10.1063/1.2950209>
8. Janne Wallenius, "Nitride Fuels," in *Comprehensive Nuclear Materials*, 2nd Ed., Konings, R.J.M. (Ed.), Elsevier 2020, pp. 41–54.
9. Walter R. Witzke, "COMPOSITIONAL EFFECTS ON MECHANICAL PROPERTIES OF HAFNIUM-CARBIDE-STRENGTHENED MOLYBDENUM ALLOYS," NASA TM X-3239, NASA Lewis Research Center, May 1975.
10. L.B. Lundberg, "A Critical Evaluation of Molybdenum and Its Alloys for Use in Space Reactor Core Heat Pipes," LA-8685-MS, UC-38, Los Alamos Scientific Laboratory, January 1981.
11. W.D. Klopp, "Technology Status of Molybdenum and Tungsten Alloys," Chapter 42, *Space Nuclear Power Systems, Vol. 2*, M.S. El-Genk and M.D. Hoover, Eds., Orbit Book Co., 1984, pp. 359-370.
12. Dave Wootan, et al., "Isotope Production Test in the Fast Flux Test Facility," *Proceedings of LMR: A Decade of LMR Progress and Promise*, Washington, D.C., November 11-15, 1990, ANS, 1990.

## Appendix A – A Molten-Lead Loop for Material and Component Testing

JJ Jenks, Harold Adkins, Carl Enderlin  
PNNL-Nuclear Sciences Division

### Introduction

The U.S. has been a leader in liquid-metal reactor research for the better part of a century. Although most of that effort has been focused on sodium-cooled fast reactors (SFR), there has also been work on lead (Pb) cooled fast reactors. Until recently, lead has not been chosen for use in reactors in the U.S. due to corrosion issues. As such, Russia has been the leader in lead cooled reactors and has deployed them in their Alpha-class submarines. Since then, they have designed the BREST; a 1.2 GWe lead cooled reactor for commercial power generation. As the BREST has been marketed worldwide, the U.S. has devoted more research into Pb-cooled reactor technology [1].

There are several advantages to using lead cooled reactors. Lead coolant absorbs fewer fast neutrons than other coolants, allowing for a more sustainable fuel cycle. In addition, phase change is not a major concern due to its boiling point of 1740 °C, lending itself well to VHTRs and other advanced reactor concepts.

Hydromine has envisioned the use of Lead Cooled Fast Reactors (LFRs) on the scale of small modular and microreactors for safe, long-term, cost-effective energy for remote areas and propulsion of commercial vessels. During their first phase, they developed the LFR-TL-5 (5 MWe,  $T_{\text{core}}=420$  °C) for remote sites with a target deployment in the later part of this decade. The second phase will deploy more power (tens of MWe,  $T_{\text{core}}=530$  °C) and will be specific for marine propulsion with a target year of 2030. The final phase will deliver a 200 MWe, 530 °C reactor (LFR-AS-200) later in 2030. Phase 2 and 3 require new materials to be qualified. The benefits of Hydromines' LFR technology over existing Sodium Fast Reactors (SFRs) include a smaller footprint by 4X, no intermediate loops (Pb is poor absorber of fast Neutrons), a compact primary system and no LOCA.

The challenge for LFRs involve corrosion prevention, and therefore special attention must be given to the materials used in construction of all components exposed to molten lead. In order to test various components, PNNL will design and construct a test facility that is capable of circulating molten lead at temperatures in the range of interest (420-600 °C) with the anticipation of reaching maximum temperatures over 1000 °C. A versatile test-section will be used that can incorporate all components exposed to lead in the LFR. The test section will be capable of testing multiple components at a time to reduce total time required for testing.

## Core Capabilities

PNNL has a long history of developing full-scale fluid systems for DOE, the NRC and private industry. Most recently these systems have included a loop designed and constructed to study accidental spray release of nuclear waste at high flow (300 gpm) and pressure (380 psig) as shown in Figure A.1. [2]

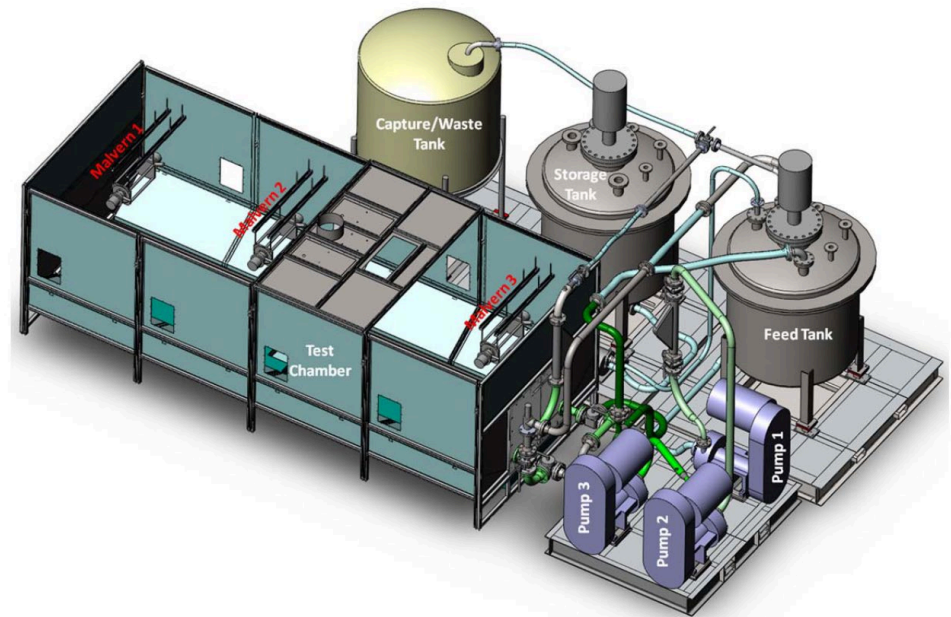


Figure A.1. Large-scale spray release test facility used at PNNL

The same team developed the Multiphase Transport and Evaluation Loop (MTEL) that has been used for testing non-invasive flow measurement devices used on nuclear waste streams [3] and was subsequently retrofitted for autonomous operational cycle testing of 3-inch nuclear waste transfer valve used for double-valve isolation as shown in Figure A.2. This system evaluated valve degradation (e.g., valve leakage and operating performance) as a function of operating cycles.

In addition to experimental capabilities, PNNL's Computational Fluids and Mechanics team has expertise in designing and simulating mechanical, heat, mass and fluid phenomena associated with nuclear components, with several decades of modeling nuclear reactors, storage and waste transfer. The team uses high performance computers (HPCs) located at the PNNL Institutional Cluster (PIC) on campus to run parallel simulations for rapid solution convergence.

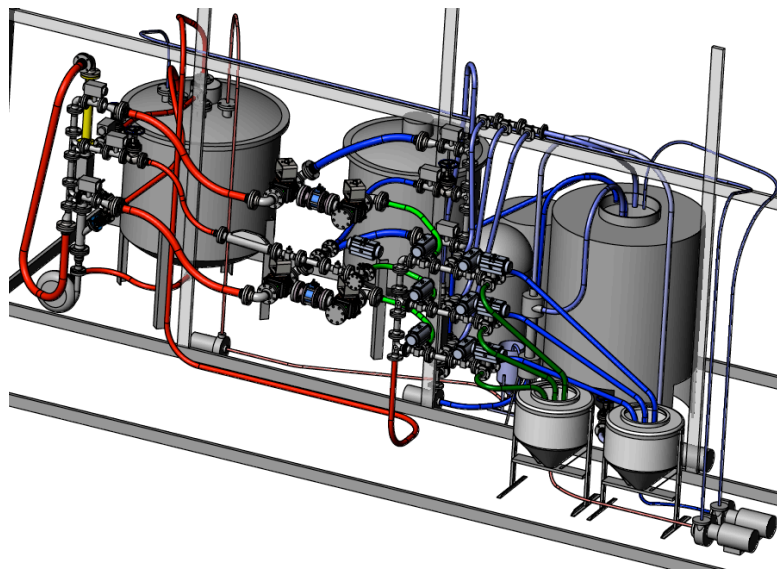


Figure A.2. Full scale dual valve isolation cycle test facility used at PNNL

PNNL has an extensive history in the area of corrosion testing and development of advanced manufacturing technologies. This combination has helped build an expertise in corrosion not

just related to materials and their operating environments, but the impact of component and system fabrication on corrosion.

## Test Facility Design and Construction

PNNL will design and construct a molten lead loop to test the efficacy of components, materials and sensors necessary for the development and demonstration of a lead coolant fast reactor (LFR). The facilities will be capable of heat inputs from  $\text{kW}_t$ - $\text{MW}_t$  scales depending on requirements for the specific units under test. The closed loop will consist of modular components that can be easily modified to accommodate various test sections. A minimum of two loops will be required for small scale ( $\text{kW}_t$ ) and large scale ( $\text{MW}_t$ ) testing. Each of these loops will use either electromagnetic (EM) pumps or the same STSG-pumps used by Hydromine as the motive force for molten lead fluid transport. Additionally, PNNL has built upon over 30 years of experience building and testing electromagnetic Annular Linear Induction Pumps that have been used for space nuclear power systems developed at NASA as shown in Figure A.3[4].

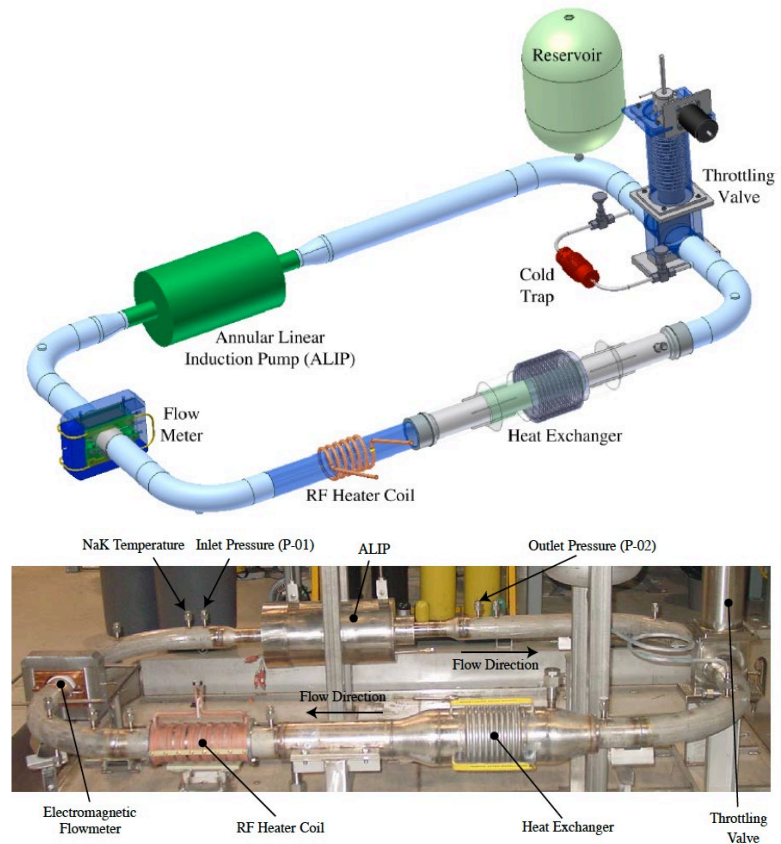


Figure A.3. Test loop used at NASA-Marshall Space Flight Center incorporating PNNL developed ALIP

The molten lead loop will be autonomously controlled using a dedicated data acquisition and control system (DACS) comprised of programmable logic control (PLC) input/output modules. Loop operation and real-time values for all data (Pressure, temperature, flow,  $\text{O}_2$  concentration, valve-position, off-gas composition etc.) will be recorded and displayed on large screen monitors and manual startup and control will occur via a touch-screen human machine interface (HMI). Flow rates will be measured by ultrasonic flow-meters capable of measuring bulk fluid velocities in the range of 0-5 m/s. A combination of in-line radiant and electrical resistant heaters will be used to maintain the fluid temperature at a minimum of  $550\text{ }^\circ\text{C}$  and up to  $1000\text{ }^\circ\text{C}$ . Molten lead will flow into the loop from primary and secondary melt tanks. Oxygen levels will be monitored using probes originally developed by LANL that use yttria-stabilized zirconia (YSZ) electrolyte and reference electrodes.  $\text{O}_2$  levels will be controlled by injection of argon and hydrogen or hydrogen/water and hydrogen/oxygen mixtures. An autonomous fault detection, isolation and recovery (FDIR) algorithm will be developed to maintain critical parameters

(temperature, pressure, flow and oxygen concentration) in the loop. The program will first generate an alert condition and attempt to autonomously rectify any discrepancies from setpoint ranges to maintain loop operation. In any event where the measured value is outside of the acceptable limits, the loop will automatically revert to safe operation mode by controlling and/or shutting down the heat input and pump. Off-gas will occur via a dedicated system that will remove Pb-oxides, particulates and reactive gases to prevent discharge to the environment. The system will include sintered metal filters, activated alumina and HEPA filters and vacuum pumps necessary to purge the loop prior to operation. Necessary heat rejection equipment will be incorporated.

## Cost estimate (ROM)

A rough order of magnitude is provided based on costs estimated for a similar system[1]. For MW scales PNNL will require a dedicated facility due to loop size and power requirements. An estimate for MW scales requires a more rigorous analysis with special attention to available lab space (vs new construction) and facility power modifications.

It is estimated that the design and construction cost for the aforementioned system will be \$12.5K/kW<sub>t</sub>. A small-scale system defined as 100 kW<sub>t</sub> would cost \$1.3M. Inclusion of an ALIP pump would bring that cost closer to \$1.6M. A large-scale system defined as 1MW<sub>t</sub> would cost roughly \$10M-\$13M for design and construction and would be proportionally higher for larger systems. Note that this doesn't include any building construction or modification costs that may be required for a large-scale system.

## REFERENCES

1. Khericha, S., Lead Coolant Test Facility Technical and Functional Requirements, Conceptual Design, Cost and Construction Schedule. 2006, INL: Idaho Falls, ID.
2. Bontha J.R., P.A.G., D.E. Kurath, H.E. Adkins, C.W. Enderlin, J.J. Jenks et al., Experimental Challenges and Successes in Measuring Aerosol Concentrations at Prototypic Spray Conditions Encountered at the Hanford Waste Treatment and Immobilization Plant - 13327., in Waste Management Symposia (WM2013): International Collaboration and Continuous Improvement. 2013.
3. Denslow, K.M.J., Jeromy WJ; Bontha, Jagannadha R.; Adkins, Harold E.; Burns, Carolyn A.; Schonewill, Philip P. et al., Hanford Tank Farms Waste Certification Flow Loop Phase IV: PulseEcho Sensor Evaluation. 2011, PNNL: Richland, WA. p. 83.
4. Kurt A. Polzin, M.S., J. Boise Pearson, Kenneth Webster, Thomas Godfroy, Harold E Adkins Jr., James E. Werner, Performance of an Annular Linear Induction Pump with Applications to Space Nuclear Power Systems, in International Energy Conversion Engineering Conference. 2010: Nashville, TN.

## Appendix B – Efficiencies Comparison

Figure B.1 shows a plot of Carnot, Brayton, and NTPV efficiencies in addition to the Landsberg limit. Brayton and NTPV efficiencies were used in calculating overall power component sizes shown in the size/weight figures above.

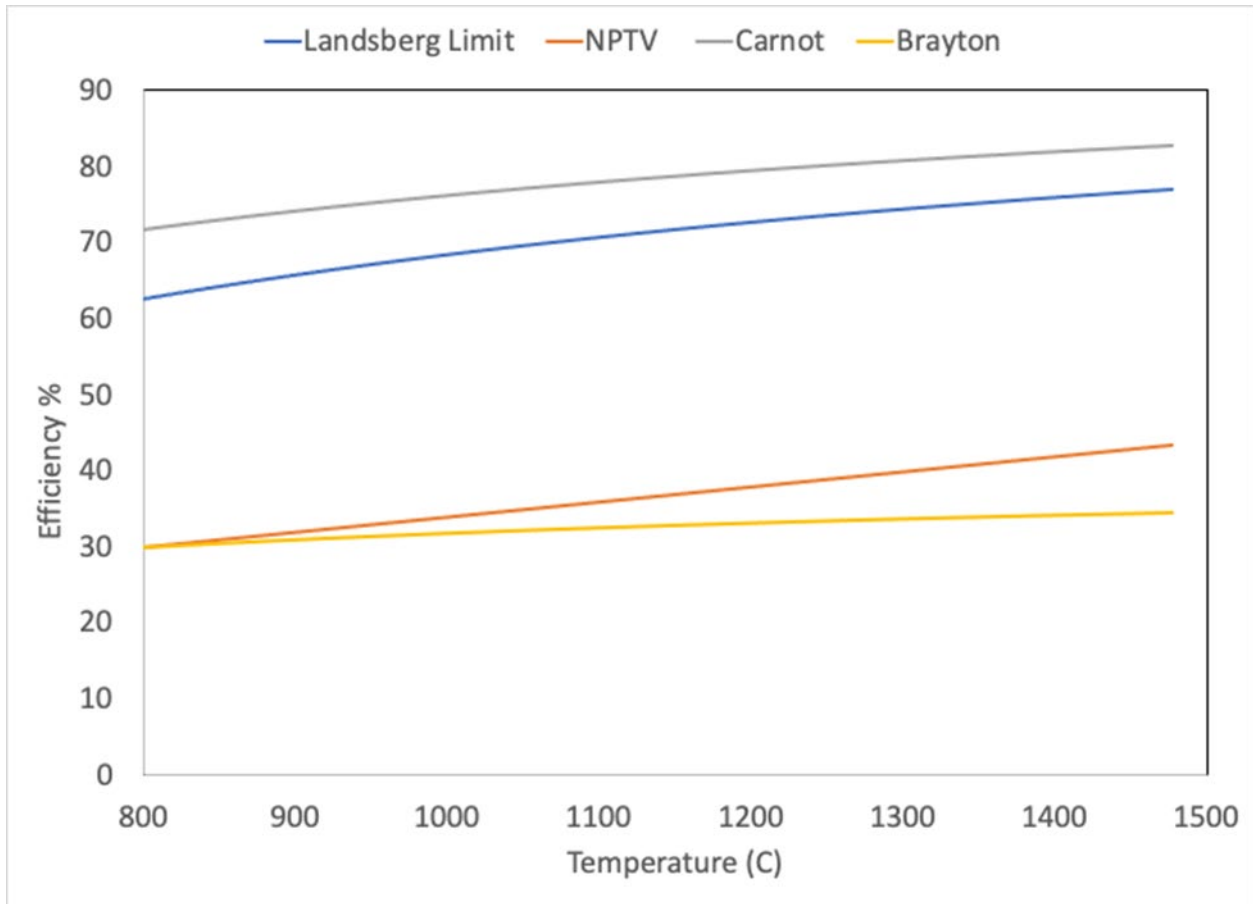


Figure B.1. NTPV Efficiency is based on optical properties with a maximum equivalent to the Landsberg limit (lower than the Carnot Limit). Brayton System maximum efficiency is defined by the Carnot limit.



# Pacific Northwest National Laboratory

902 Battelle Boulevard  
P.O. Box 999  
Richland, WA 99354  
1-888-375-PNNL (7665)

***[www.pnnl.gov](http://www.pnnl.gov)***